Progress In Electromagnetics Research, PIER 81, 41–59, 2008

A NOVEL METHOD FOR TESTING ULTRA WIDEBAND ANTENNA-FEEDS ON RADIO TELESCOPE DISH ANTENNAS

S. Joardar

Tata Institute of Fundamental Research
Giant Meterwave Radio Telescope
Narayagaon, Pune-410504, Maharashtra, India

A. B. Bhattacharya

Department of Physics
University of Kalyani
Nadia-741235, West Bengal, India

Abstract—A prototype of dual polarized ultra wideband antenna-feed was fabricated (200 MHz–2000 MHz) for usage in low frequency radio astronomy at the GMRT (Giant Meterwave Radio Telescope). The feed was mounted on one of the GMRT dish antennas and tested using signals from the radio galaxy Cygnus A and zenith sky. Modeling of the GMRT dish with the antenna-feed mounted at its focus has been done. With the use of simulated radiation patterns of the antenna-feed and the measured results, the system independent deflections at various frequencies were computed. The performances of the GMRT dish with present mesh and RMS (root mean square) efficiencies have been studied. Performance of the GMRT dish with 100% mesh and RMS efficiencies were computed. Future guidelines of ultra wideband antenna-feed design for GMRT have been indicated. Improvements of the GMRT dishes have also been suggested.

1. INTRODUCTION

Today, radio astronomy is attempting to expand its scope in observations by passively utilizing the temporary free frequency bands owned by other users. This requires ultra wideband antenna-feeds

mounted at the focus of radio telescope (dish reflector) antennas. Several ultra wideband antennas that shows the possibility of being used as antenna-feed with parabolic reflectors has been reported [1–8]. However, the actual testing of any of these on radio telescope antennas has not been reported so far. In this paper we discuss a method and its application for radio astronomical testing of telescope antennas. We have used a step-lane reflector based ultra wideband antenna-feed (200 MHz–2000 MHz, 9 dBi gain) [2], which was mounted on a GMRT[†] dish for this purpose.

The antenna design and applications always involve several optimization processes, especially when used as arrays, as in radio telescopes. These are applied side by side with the measurement results. Few of the recent optimization techniques proposed by the antenna designers are listed in references [9–17]. Depending on the structure of the reflector antennas and the antenna-feed configurations, the field analysis also needs to be done. A few such methods are listed in references [18–20]. However, the classical tests of antenna-feeds of radio telescope are based on deflection obtained by observing an astronomical source against the sky [21, 22]. These tests are unavoidable and could be extended for judging the system-independent performance of the telescope antenna. The signals from the background sky and astronomical source need to be measured at all frequencies supported by the antenna-feed. The incremental temperature of the source against the background sky could be used to estimate the coupling between the source and the antenna. In order to study purely the antenna properties, a method have been developed to remove the system dependent properties. It uses the measured spectra of an astronomical source and the sky (using the telescope antenna setup) along with the system characteristics as its inputs. The test setup for these measurements (using the antenna-feed on a GMRT dish) and the system characteristics are presented in Section 2. The spectra thus obtained for usage in the analysis is presented in Section 3. The analysis method consists of three parts: (i) approximate estimation of antenna aperture efficiency, (ii) detailed performance estimation of the antenna-feed on a real dish and (iii) detailed performance estimation of the antenna-feed on an ideal dish. The first part gives a rough understanding of the dish and is presented in Section 4. The second part estimates a system independent performance of the antenna-feed on the available dish and is presented in Section 5. The third part estimates the performance of the antenna-feed if the dish had a smooth surface, and is presented in Section 6. Based on the analysis results, the pros and cons of the

[†] Giant Meterwave Radio Telescope, situated about 80 km North of Pune, India.

GMRT dishes have been thoroughly estimated. Certain changes in the GMRT dish and the antenna-feed have been suggested for improving the performance of the radio telescope.

2. SETUP AND GMRT SYSTEM RESPONSE APPLIED FOR TESTING THE ULTRA WIDEBAND ANTENNA-FEED

The antenna-feed was mounted on one of the GMRT telescope dishes and tested for an extra terrestrial radio source. The details of the setup used for the radio astronomical testing is shown in Fig. 1. Part (a) of the figure explains the details of a GMRT antenna along with its regular antenna-feeds. There are three different antenna-feeds for observations at different frequency bands, and an antenna-feed for dual frequency observation. All of them are suspended by four arms near the focus of the dish known as *quadripod arms*. For any astronomical observation, only one of the feeds is positioned at focus of the dish using a remotely controlled feed positioning system. Part (b) shows the mounting position of the ultra wideband feed on the GMRT dish. Part (c) shows the block diagram for astronomical *onsource* and *offsource* test setup. Each of the antenna-feed outputs (both polarizations) is sent to the respective LNA followed by the GMRT receiver system enclosed within the common box. The power from the antenna-feeds after sufficient amplifications are sent to a spectrum analyzer kept inside the antenna shell. Part (d) shows the setup for measurement of system characteristics. The inputs of the LNAs are terminated with matched loads and the system responses are plotted in black as shown in Fig. 2. Part (a) shows the terminated response and calculated gain over 300 MHz to 375 MHz band. Part (b) shows the same over 600 MHz to 2000 MHz. The system gain G_{sys} has been approximately calculated from the terminated characteristics using Equation (1), where, $k = 1.38 \times 10^{-23}$ J/K (Boltzmann constant), $T_{rec} = 50^{\ddagger}$, $T_{load} = 300$ K and $\triangle f = 300000$ Hz is the resolution bandwidth. The gain plots are also shown in Fig. 2 in gray.

$$G_{sys} = \frac{P_{out}}{k(T_{rec} + T_{load})\Delta f} \tag{1}$$

‡ The LNA temperature is about 41°K. The temperature contribution by the RF-cables (especially between LNA and antenna-feed), connectors and other electronic systems is about 10°K.

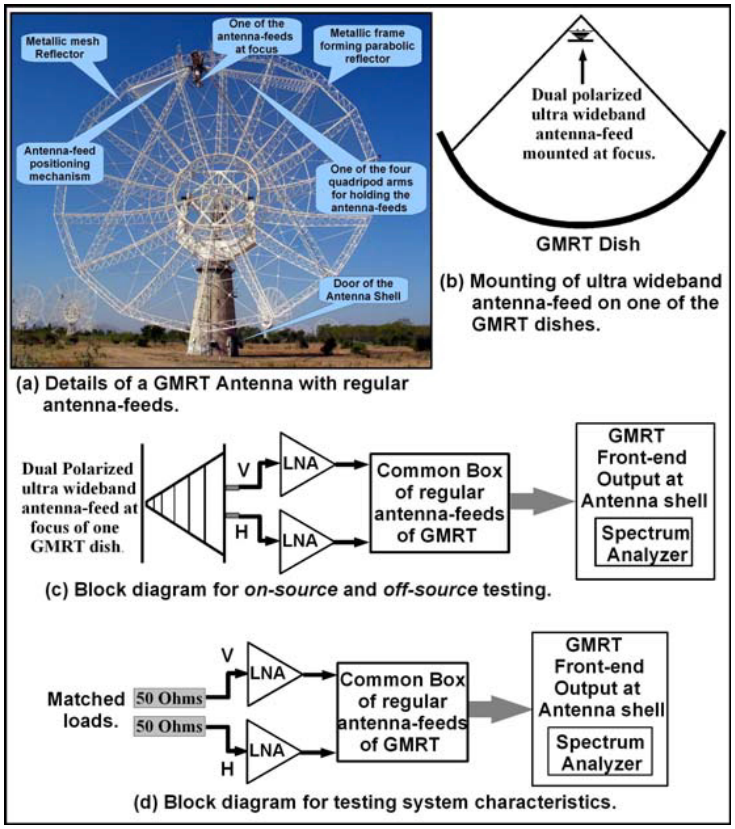

Figure 1. Details of the setup used for radio astronomical testing of the ultra wideband antenna-feed on a GMRT dish antenna, (a) physical details of a GMRT dish antenna, (b) mounting of the ultra wideband antenna-feed, (c) block diagram of *onsource* and *offsource* test setup, (d) setup for measurement of system characteristics.

3. RADIO ASTRONOMICAL MEASUREMENTS OF CYGNUS A AND SKY

The signals obtained from the radio galaxy Cygnus A and sky using the ultra wideband antenna-feed mounted at the focus of one of the GMRT antennas are presented in this section. Results from only one polarization are plotted, since they closely resemble with the results of the other polarization. Measurements were made between 300 MHz to 375 MHz and then from 600 MHz to 2000 MHz, depending on the available supporting instruments like LNA, etc. from the

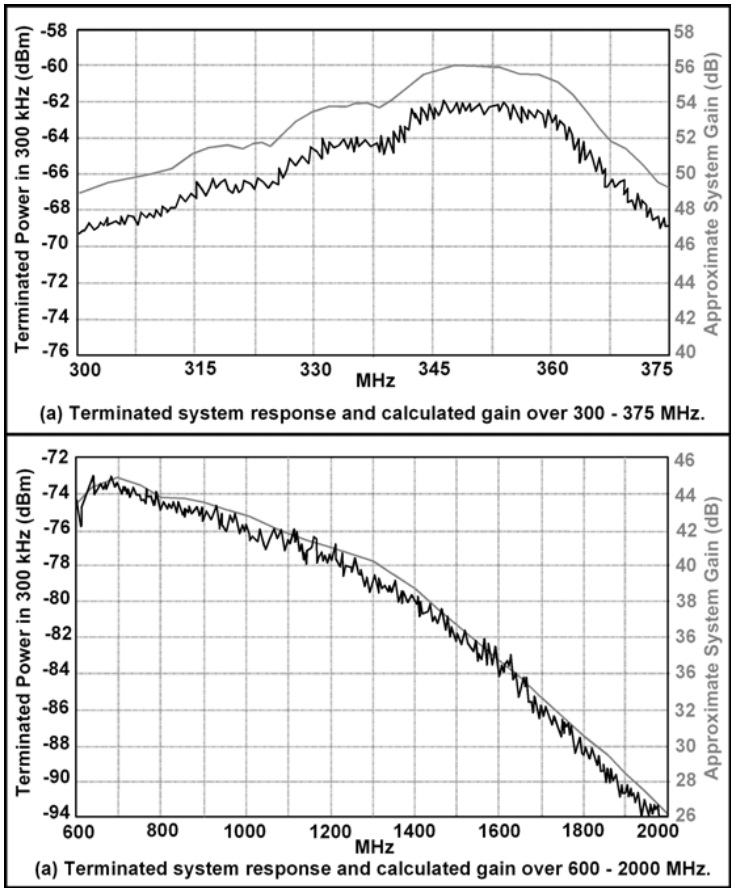

Figure 2. Terminated system characteristics of GMRT (black curves) and computed system gains (gray curves).

GMRT. Figs. 3, 4 and 5 show the measured signals received at the GMRT receiver system output using the ultra wideband antenna-feed. Signals represented in black and gray are obtained by pointing the GMRT dish toward Cygnus A and zenith (sky) respectively. Some narrowband interferences from distant radio broadcasts are seen. Strong interferences from GSM are also seen within 800–1000 MHz and 1800–2000 MHz range. Note that the ratio of the signals from Cygnus A to sky decreases with increase in frequency. The GMRT dishes are designed for operation up to 1420 MHz. There are several factors affecting the telescope response, especially at higher frequencies. These could be broadly listed as (a) the flux density of Cygnus decreases with

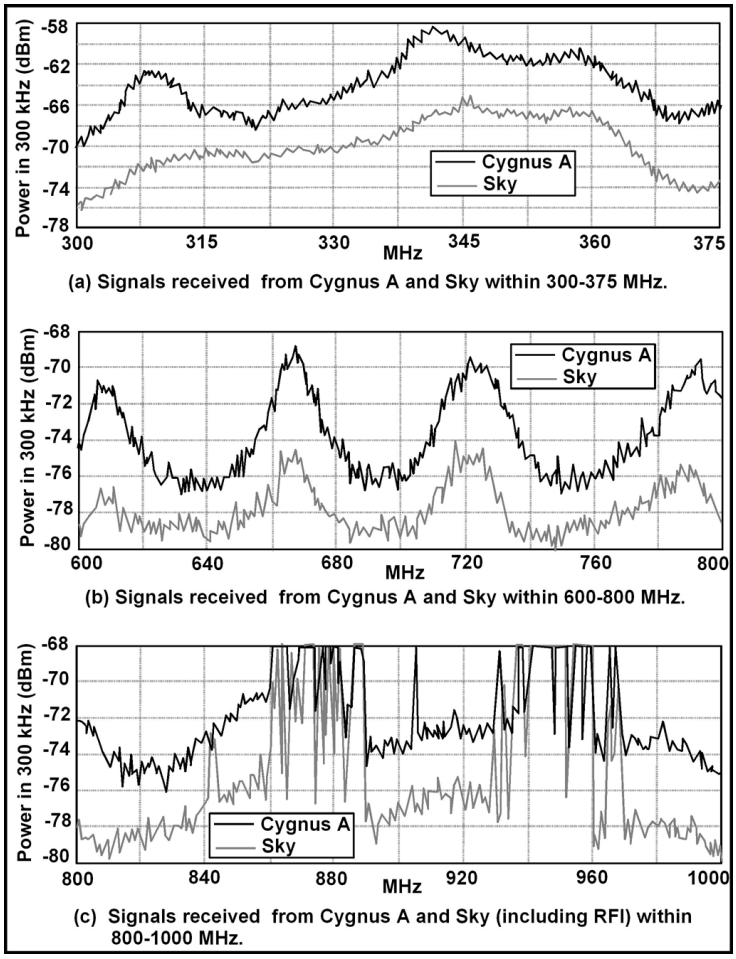

Figure 3. Signals received with GMRT receiver system using the ultra wideband antenna-feed mounted at the focus of one of the GMRT dishes. Signals represented in black and gray are obtained by pointing the GMRT dish toward Cygnus A and zenith (sky) respectively, (a) signals received from Cygnus A and sky within 300–375 MHz, (b) signals received from Cygnus A and sky within 600–800 MHz, (c) signals received from Cygnus A and sky within 800–1000 MHz. Strong interferences from GSM stations are seen.

frequency, (b) the leakage of the ground temperature into the antenna-feed though the mesh of the GMRT dishes increases with frequency, i.e., the mesh efficiency of GMRT dishes decreases with increase in

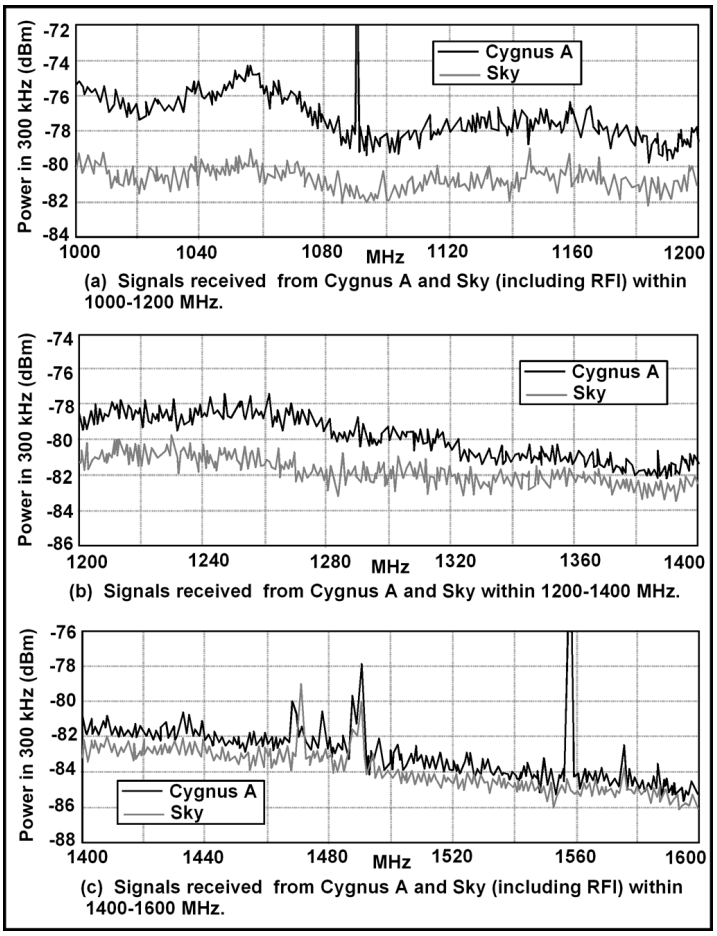

Figure 4. Signals received with GMRT receiver system using the ultra wideband antenna-feed mounted at the focus of one of the GMRT dishes. Signals represented in black and gray are obtained by pointing the GMRT dish toward Cygnus A and zenith (sky) respectively. Some narrowband interferences from distant transmitters are also seen, (a) signals received from Cygnus A and sky within 1000–1200 MHz, (b) signals received from Cygnus A and sky within 1200–1400 MHz, (c) signals received from Cygnus A and sky within 1400–1600 MHz,

frequency, (c) the surface of the GMRT dishes are less uniform at higher frequencies, i.e., RMS efficiency decreases with frequency, (d) the receiver temperature possibly affects the antenna temperature at higher frequencies since the temperature of the sky and Cygnus

A reduces at higher frequencies, (e) the temperature contribution from ground due to beam spillover tends to dominate over the sky temperature at higher frequencies. We shall investigate them in details in the upcoming sections.

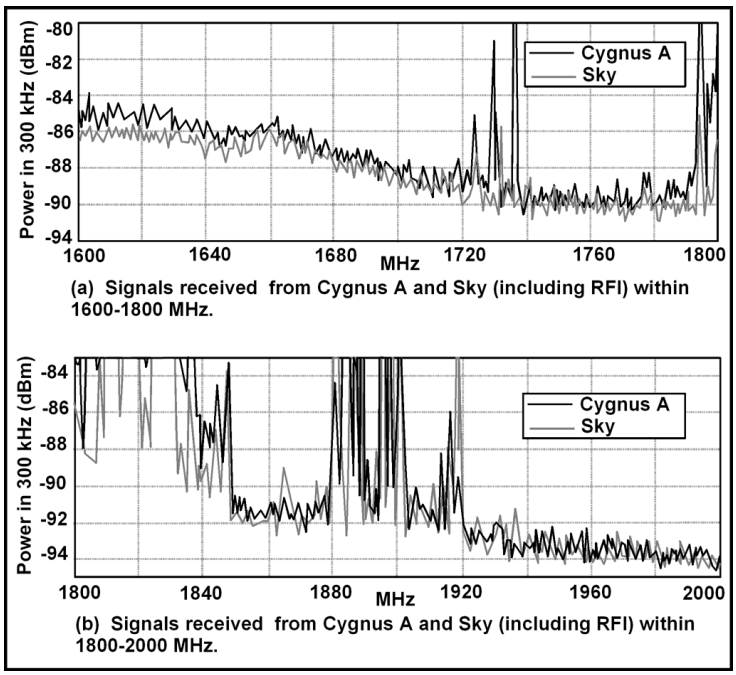

Figure 5. Signals received with GMRT receiver system using the ultra wideband antenna-feed mounted at the focus of one of the GMRT dishes. Signals represented in black and gray are obtained by pointing the GMRT dish toward Cygnus A and zenith (sky) respectively. Strong interferences from GSM stations are seen, (a) signals received from Cygnus A and sky within 1600–1800 MHz, (b) signals received from Cygnus A and sky within 1800–2000 MHz.

4. APPROXIMATE ESTIMATION OF ANTENNA APERTURE EFFICIENCY ON AN EXISTING GMRT DISH

The f/D ratio of the GMRT antennas is 0.412, where f is the focal length and D is the diameter or the dish. From the geometry shown in Fig. 6, the focal length f calculated using Equation (2) is 18.54 m,

with D as 45 m[§]. Using Equation (3) the depth d of the dish is found to be 6.83 m. The total edge illumination beam angle θ_d calculated using Equation (4) is found to be approximately 125°. Comparing the radiation patterns of the ultra wideband antenna-feed [2] with Fig. 6, it may be observed in general that more than 87% of the beam illumination is towards the parabolic reflector. The Remaining 13% appears as sidelobes and backlobes. When the paraboloid looks towards the zenith, the ground spillover angle $2\theta_s = \theta_{s1} + \theta_{s2}$ is nearly $180° - 125° = 55°$. Assuming that the sidelobes and backlobes are on an average uniformly distributed within rest of the angle $2\theta_s + \theta_b$, the contribution to antenna temperature could be roughly estimated[‖]. To be noted that certain portion of the back-sidelobes are reflected/diffracted back towards the ground due to the arrangement of holding the antenna-feed at the focus of the GMRT dish (shown in Fig. 6(b)) and also due to the quadripod arms (shown in Fig. 1(a)). Since the GMRT dishes use metallic mesh instead of a solid surface, there occurs a mesh leakage which increases with frequency. The RMS efficiency (due to surface irregularity) of the GMRT dish also decreases with frequency. The taper efficiency is considered optimum if the majorlobe falls by 10 dB at the edge of the dish [22]. This has been the criterion for the present prototype of ultra wideband antenna-feed design. Since the antenna-feed is of frequency independent type, we assume the taper efficiency to be identical at all frequencies. The aperture efficiency is the product of taper efficiency, spillover efficiency, mesh efficiency, RMS efficiency with antenna-feed gain efficiency, and is expressed in Equation (5)[¶] [23]. The effective gain of the antenna (dish plus antenna-feed) could be calculated using Equation (6). The effective half power beamwidth could be calculated next using Equation (7) [22]. Table 1 lists the values of approximate estimation of all efficiencies, effective gains and effective half power beam widths.

$$f = 0.412D \tag{2}$$

$$d = \frac{D^2}{16f} \tag{3}$$

$$\theta_d = 2\tan^{-1}\left(\frac{D/2}{f-d}\right) \tag{4}$$

$$\eta_{aperture} = \eta_{taper}\eta_{spillover}\eta_{mesh}\eta_{rms}\eta_{ant} \tag{5}$$

[§] The diameter of any GMRT dish is 45 m.

[‖] In later sections, the temperature contributions have been estimated in more details using individual radiation patterns at different frequencies.

[¶] Assuming phase efficiency to be 100%.

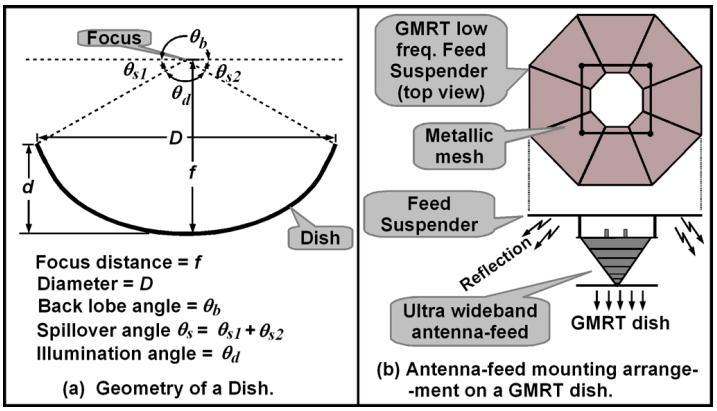

Figure 6. Estimation of ground spillover and backlobe angles, (a) the geometry of a simple parabolic dish, (b) mounting arrangement of the ultra wideband antenna-feed on a GMRT dish.

Table 1. Rough estimation of aperture efficiency, effective gain and effective half power beamwidths using ultra wideband feed on a GMRT dish.

Frequency (MHz)	233	327	610	1000	1200	1400
η_{taper}(antenna-feed)	0.78	0.78	0.78	0.78	0.78	0.78
η_{spill}(antenna-feed)	0.6473	0.8692	0.8035	0.8938	0.9152	0.8743
η_{mesh}(GMRT dish)*	0.999	0.998	0.991	0.943	0.941	0.940
η_{rms}(GMRT dish)*	0.992	0.986	0.948	0.88	0.835	0.78
η_{ant}(antenna-feed)	0.98	0.98	0.97	0.94	0.93	0.91
Aperture efficiency	0.49	0.6538	0.5711	0.5438	0.5216	0.4550
G_{eff}(dBi)	27.77	31.97	36.80	40.88	42.28	43.02
$\theta_{eff\,HPBW}$(degree)	8.17	5.04	2.89	1.8	1.53	1.41

*For more details see reference [23].

$$G_{eff} = \eta_{aperture} \left(\frac{\pi D}{\lambda}\right)^2 \tag{6}$$

$$\theta_{eff\,HPBW} = \sqrt{\frac{40000}{G_{eff}}} \tag{7}$$

5. DETAILED PERFORMANCE ESTIMATION OF ULTRA WIDEBAND ANTENNA-FEED ON AN EXISTING GMRT DISH

Since the GMRT is functional up to 1420 MHz, the performance of the ultra wideband antenna-feed has been evaluated between 300 MHz to 1600 MHz. The contributions to antenna temperature could be visualized from Fig. 7(a) and (b) respectively for the pointing toward sky and Cygnus A. The angles θ_d, $\theta_{s1}+\theta_{s2}$, $\theta_{b1}+\theta_{b2}$ and θ_{b3} respectively represent the illumination covering angles in one dimension for dish, spillover, backlobes directly looking toward sky, and backlobes reflected back to ground by GMRT's feed suspender. The phase efficiency has been assumed to be unity. With reference to Fig. 7(a), the antenna temperature with the GMRT dish pointing toward zenith sky is expressed as in Equation (9), where a_x is the ratio of integrated radiation patterns as expressed in Equation (8). The quantities $A_E(\theta)$ and $A_H(\phi)$ represent the radiation patterns in two orthogonal planes each bisecting the major lobe of the antenna-feed into two halves. Thus the extents of θ and ϕ lie between 0° and 360°. If the beam patterns in both the planes are more or less similar, a_x may be approximately calculated by substituting $A_E(\theta)$ and $A_H(\phi)$ with the mean of the two in Equation (8). It is a dimensionless quantity having a maximum value of unity. It represents the power distribution of the antenna-feed's beam pattern within different angular extents in both planes. Table 2 lists the values of a_x using the mean of the theoretically computed E and H radiation patterns. The symbol η stands for efficiency with its subscript describing its type. With reference to Fig. 7(b), the antenna temperature with the GMRT dish pointing toward the radio galaxy Cygnus A is expressed as in Equation (10), where, Jy_{Cygnus} is the flux density of Cygnus A in jansky and κ is the coupling factor in °K/Jy for converting this flux density into equivalent temperature contribution to the antenna-feed. The flux density of Cygnus A [24, 25] and temperature of the sky [22] against frequency is shown in Fig. 8. The value of κ has been computed from the measured results as explained next.

$$a_{(\theta_2-\theta_1)(\phi_2-\phi_1)} = \left[\frac{\int_{\phi_1}^{\phi_2}\int_{\theta_1}^{\theta_2} A_E(\theta)A_H(\phi)d\theta d\phi}{\int_0^{2\pi}\int_0^{2\pi} A_E(\theta)A_H(\phi)d\theta d\phi} \right], \text{ where } \phi_1 = \theta_1,\ \phi_2 = \theta_2 \tag{8}$$

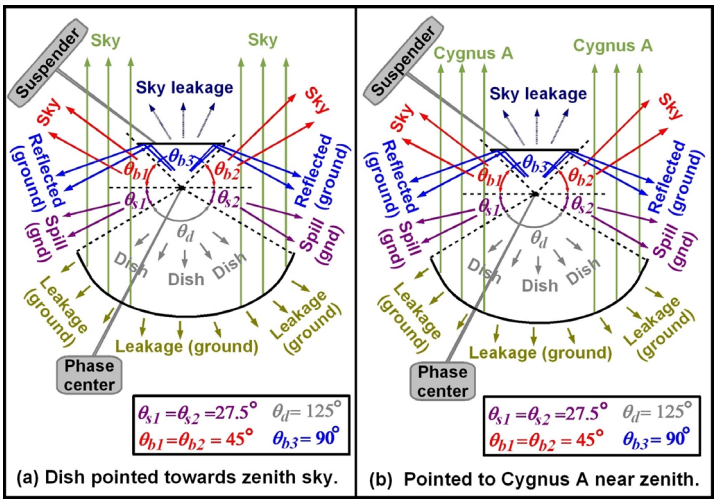

Figure 7. Estimation of signal pickup from sky, Cygnus A and ground, (a) signal pickup from various sources with GMRT dish pointed to the zenith (sky), (b) signal pickup from various sources with GMRT dish pointed to radio galaxy Cygnus A near zenith.

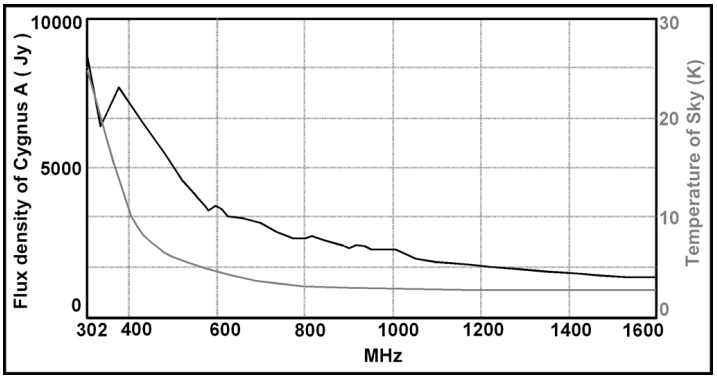

Figure 8. Variation of flux density of Cygnus A (black curve) and temperature of sky (gray curve) against frequency.

$$
\begin{aligned}
T_{ant(ZenSky)} &= \eta_{ant}\left\{T_{SkyPickup} + T_{GndPickup}\right\} \text{ where,} \\
T_{SkyPickup} &= T_{sky}\left\{a_d\eta_{mesh}\eta_{rms} + a_{b1} + a_{b2} + a_{b3}\left(1-\eta_{mesh}\right)\right\} \\
T_{GndPickup} &= T_{gnd}\left\{a_{s1} + a_{s2} + a_d\left(1-\eta_{mesh}\right) + a_{b3}\eta_{mesh}\right\} \qquad (9)
\end{aligned}
$$

$$\begin{aligned} T_{ant(Cygnus)} &= \eta_{ant}\left\{T_{CygPickup} + T_{SkyPickup} + T_{GndPickup}\right\} \text{ where,} \\ T_{CygPickup} &= \kappa Jy_{Cygnus} a_d \eta_{mesh} \eta_{rms} \\ T_{SkyPickup} &= T_{sky}\left\{a_{b1} + a_{b2} + a_{b3}\left(1 - \eta_{mesh}\right)\right\} \\ T_{GndPickup} &= T_{gnd}\left\{a_{s1} + a_{s2} + a_d\left(1 - \eta_{mesh}\right) + a_{b3}\eta_{mesh}\right\} \end{aligned} \quad (10)$$

Table 2. Computed values of a_x and κ(°K/Jy) is based on theoretical radiation patterns and measurements.

Freq. (GHz)	a_d (×1)	a_{s1} ($\times 10^{-3}$)	a_{s2} ($\times 10^{-3}$)	a_{b1} ($\times 10^{-3}$)	a_{b2} ($\times 10^{-3}$)	a_{b3} (×1)	κ (°K/Jy)
0.302	0.8151	0.0778	0.0737	0.7676	0.7858	0.0255	0.0563
0.400	0.6824	0.2595	0.2850	1.3750	1.5784	0.0669	—
0.500	0.8138	0.1436	0.1902	0.3581	0.4227	0.0343	—
0.600	0.7590	0.0633	0.0457	1.6069	1.7185	0.0339	0.1100
0.700	0.8779	0.0540	0.0626	0.2772	0.2741	0.0157	0.0510
0.800	0.8935	0.0166	0.0203	0.2129	0.1863	0.0188	0.2278
0.900	0.8586	0.1529	0.1736	0.2187	0.2067	0.0204	0.1944
1.000	0.8632	0.1536	0.1430	0.2165	0.2101	0.0188	0.1652
1.100	0.8552	0.1472	0.2345	0.2765	0.1728	0.0197	0.1047
1.200	0.8907	0.0900	0.0996	0.1370	0.1384	0.0146	0.1036
1.300	0.9192	0.0601	0.0667	0.0857	0.0777	0.0087	0.1248
1.400	0.8114	0.2288	0.1979	0.2953	0.2427	0.0392	0.1076
1.500	0.5663	0.6181	0.6874	0.3838	0.4304	0.1582	0.1287
1.600	0.7844	0.0300	0.1453	0.5445	0.4949	0.0525	0.0899

The incremental temperature $\triangle T$ between sky and Cygnus A for any particular frequency could be computed using Equation (11). It can be calculated from the measured results at that frequency using Equation (12), where P_{Cygnus} and P_{sky} are the powers received at the output of the system (using spectrum analyzer inside the antenna shell) having pointed the GMRT dish to Cygnus A and sky respectively. Equating these two equations, the value of κ can be derived as in Equation (13). Table 2 also lists the computed values of κ from the measured signals presented in Fig. 2 through 5.

$$\begin{aligned} \triangle T &= T_{ant(Cygnus)} - T_{ant(ZenSky)} \\ &= \eta_{ant}\eta_{msh}\eta_{rms}a_d\left(\kappa Jy_{Cygnus} - T_{sky}\right) \end{aligned} \quad (11)$$

$$\triangle T = \frac{P_{Cygnus} - P_{sky}}{k \triangle f G_{sys}} \tag{12}$$

$$\kappa = \left[\frac{P_{cygnus} - P_{sky}}{k \triangle f a_d \eta_{ant} \eta_{mesh} \eta_{rms}} + T_{sky} \right] \frac{1}{Jy_{Cygnus}} \tag{13}$$

The antenna temperature with GMRT dish pointing to zenith sky could be obtained from Equation (9). Having calculated κ for different frequencies, the antenna temperatures with GMRT dish pointed to Cygnus A could be derived from Equation (10) using the flux density spectrum and temperatures of zenith sky shown in Fig. 8. These two quantities, viz. $T_{ant(Cygnus)}$ and $T_{ant(ZenSky)}$ represent the temperatures that would be actually produced at the output of the ultra wideband-feed, and is independent of the system characteristics of the GMRT receiver system. These are functions of frequency since the source flux or sky temperature varies with frequency. The ratio of $T_{ant(Cygnus)}$ to $T_{ant(ZenSky)}$ is the actual gain deflection $G_{dfl(CygSky)}$ that would be produced if the antenna is moved from zenith sky to Cygnus A and is expressed in Equation (14). To estimate the deflection $G_{dfl(CygSkyRec)}$ using a receiver, the temperature of the receiver T_{rec} should also be considered as shown in Equation (15).

$$G_{dfl(CygSky)} = \frac{T_{ant(Cygnus)}}{T_{ant(ZenSky)}} \tag{14}$$

$$G_{dfl(CygSkyRec)} = \frac{T_{ant(Cygnus)} + T_{rec}}{T_{ant(ZenSky)} + T_{rec}} \tag{15}$$

6. DETAILED PERFORMANCE ESTIMATION OF ULTRA WIDEBAND-FEED ON A SMOOTH SURFACE GMRT DISH

If the GMRT dishes were considered to have good surface accuracy and no mesh transparency, the mesh efficiency and RMS efficiency becomes unity. Equations (9) and (10) could be rewritten as Equations (16) and (17) respectively.

$$\begin{aligned} T_{ant(ZenSky)} &= \eta_{ant}[T_{sky}\{a_d + a_{b1} + a_{b2}\} \\ &\quad + T_{gnd}\{a_{s1} + a_{s2} + a_{b3}\}] \end{aligned} \tag{16}$$

$$\begin{aligned} T_{ant(Cygnus)} &= \eta_{ant}[\kappa Jy_{Cygnus} a_d + T_{sky}\{a_{b1} + a_{b2}\} \\ &\quad + T_{gnd}\{a_{s1} + a_{s2} + a_{b3}\}] \end{aligned} \tag{17}$$

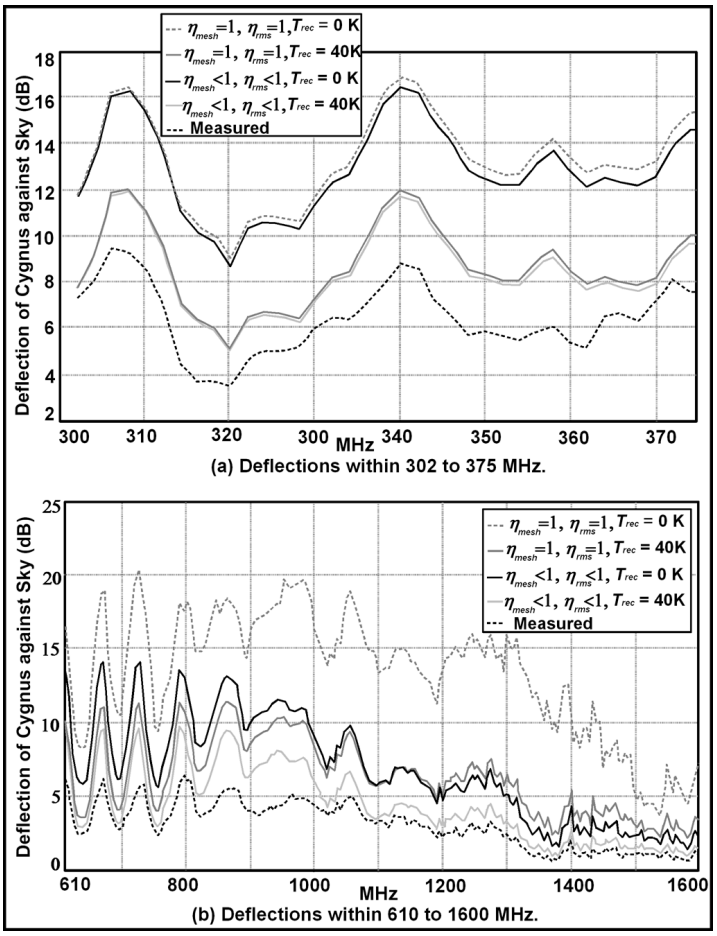

Figure 9. Results of various deflection analysis of the ultra wideband antenna-feed on a GMRT dish, (a) deflections within 300 MHz to 375 MHz, (b) deflections within 610 MHz to 1600 MHz. The measured deflection is shown in dashed black.

7. RESULTS OF ANALYSIS

The analysis was done based on the mathematical functions described before using a MATLAB script. Fig. 9 shows the results of various analysis of the ultra wideband antenna-feed on a GMRT dish. Part (a) shows the various deflections between 300 MHz to 375 MHz. Part (b) shows the various deflections between 610 MHz to 1600 MHz. Due to the log periodic nature of the antenna-feed, some ripple like

characteristics are prominently visible, especially at the low frequency end. These could be minimized very easily by increasing the width of the dipoles and reducing their number. The dashed black curve shows the measured deflection. The light gray curve represents the computed deflection from incremental temperature and coupling factor κ with a receiver temperature of 40°K. A difference is seen between the two, especially at the lower frequency end. There could be two possible reasons: (a) the modeling of the quadripod structure of the GMRT dish has not been done and (b) the minimum temperature of the sky for any frequency has been considered in our calculations[†]. The black curve shows the deflection at the output of the antenna-feed (without a receiver system). The gray curve shows the deflection if the mesh of the GMRT dish was leak-proof and had no surface irregularity, and the receiver temperature being 40°K. The dashed gray curve shows the deflection at the antenna-feed output (without a receiver system).

The optimization of a dish reflector with an antenna-feed is attained if the beam pattern of the feed falls by 10 dB at the edges of the dish [22]. The present ultra wideband antenna-feed was designed based on this optimization concept. However, as seen from Fig. 8, for low frequency radio astronomical purposes, the sky temperature saturates to about 3°K above about 800 MHz, but the signals from Cygnus A keeps decreasing and reduces by nearly 3 dB at 1600 MHz. The contribution from the ground due to spillover could significantly affect the performance of the telescope above 800 MHz since it does not decrease with frequency. The spillover may be reduced by increasing the gain of the antenna-feed, but then the dish illumination would reduce. No doubt for this reason that the GMRT telescope uses a higher gain antenna-feed (12.5 dBi) for the L-band [23] to minimize the spillover. At lower frequency end, the ground temperature does not affect much since the sky contribution is much higher.

8. SUMMARY AND CONCLUSIONS

In this article we have shown a method for radio astronomical testing of an ultra wideband antenna-feed mounted on a radio telescope dish reflector antenna. The method consists of three parts, viz. (i) approximate estimation of antenna aperture efficiency, (ii) detailed performance estimation of the antenna-feed on a real dish and (iii) detailed performance estimation of the antenna-feed on an ideal dish. The first part gives a general understanding about the performance extents of the dish. The second part uses (a) measured spectrum of the astronomical source, (b) temperature spectrum of the sky,

[†] The temperature of the sky varies reaching its maximum close to the galactic plane.

(c) frequency dependent radiation patterns of the antenna-feed and (d) frequency dependent system characteristics to find a system independent performance of the antenna-feed on the available dish. The third part estimates the performance of antenna-feed on a smooth surface perfect reflector dish of same dimension. Thus from the second part one understands the changes required in the antenna-feed for better matching with the available dish. Comparing the results of the second and third part one understands the changes required in the dish for better reception of astronomical signals. Using this method, the performance of a prototype ultra wideband antenna-feed has been tested on a GMRT dish. The theoretical radiation patterns of the antenna-feed were used for the analysis. Based on the results certain changes in the GMRT dish and the antenna-feed have been suggested.

From the analysed results it is concluded that, for frequencies below 1 GHz, the optimized dish illumination (beam pattern falling by 10 dB at the edges of the dish) could be safely used in radio astronomy. But at higher frequencies, dish illumination has to be sacrificed to avoid ground pickup. The mesh efficiency and RMS efficiencies of the GMRT dishes deteriorates significantly at higher frequencies. Improving them would additionally help in increasing the sensitivity by few dBs at the higher frequency end. The overall performance of the antenna could be further improved if the sidelobes and the backlobes of the antenna-feed are further reduced [26].

ACKNOWLEDGMENT

The authors are thankful to the editor of JEMWA and PIER and unknown reviewers of this article. The mechanical team of GMRT and their head H. S. Kale are highly acknowledged for their help in fabrication and mounting the antenna-feed on a GMRT dish.

REFERENCES

1. Olsson, R. and P. Kildal, "The eleven antenna: A compact low-profile decade bandwidth dual polarized feed for reflector antennas," *IEEE Transactions on Antennas and Propagation*, Vol. 54, No. 2, 368–375, 2006.
2. Joardar, S. and A. B. Bhattacharya, "Two new ultra wide band antenna-feeds using planar log periodic antennas and innovative frequency reflectors," *Journal of Electromagnetic Waves and Applications*, Vol. 20, No. 11, 1465–1479, 2006.

3. Dehdasht-Heydari, R., H. R. Hassani, and A. R. Mallahzadeh, "Quad ridged horn antenna for UWB applications," *Progress In Electromagnetics Research*, PIER 79, 23–38, 2008.
4. Zhang, G.-M., J.-S. Hong, and B.-Z. Wang, "Two novel band-notched UWB slot antennas fed by microstrip line," *Progress In Electromagnetics Research*, PIER 78, 209–218, 2008.
5. Hosseini, S. A., Z. Atlasbaf, and K. Forooraghi, "Two new loaded compact planar ultra-wideband antennas using deflected ground structures," *Progress In Electromagnetics Research B*, Vol. 2, 165–176, 2008.
6. Yin, X.-C., C.-L. Ruan, C.-Y. Ding, and J.-H. Chu, "A planar U type monopole antenna for UWB applications," *Progress In Electromagnetics Research Letters*, Vol. 2, 1–10, 2008.
7. Khan, S. N., J. Hu, and S. He, "Circular fractal monopole antenna for low VSWR UWB applications," *Progress In Electromagnetics Research Letters*, Vol. 1, 19–25, 2008.
8. Chen, Y.-L., C.-L. Ruan, and L. Peng, "A novel ultra-wideband bow-tie slot antenna in wireless communication systems," *Progress In Electromagnetics Research Letters*, Vol. 1, 101–108, 2008.
9. Lu, Y. Q. and J. Y. Li, "Optimization of broadband top-load antenna using micro-genetic algorithm," *Journal of Electromagnetic Waves and Applications*, Vol. 20, No. 6, 793–801, 2006.
10. Mahanti, G. K., N. Pathak, and P. Mahanti, "Synthesis of thinned linear antenna arrays with fixed sidelobe level using realcoded genetic algorithm," *Progress In Electromagnetics Research*, PIER 75, 319–328, 2007.
11. Lee, K. C. and J. Y. Jhang, "Application of particle swarm algorithm to the optimization of unequally spaced antenna arrays," *Journal of Electromagnetic Waves and Applications*, Vol. 20, No. 14, 2001–2012, 2006.
12. Chen, T. B., Y. L. Dong, Y.-C. Jiao, and F.-S. Zhang, "Synthesizes of circular antenna array using crossed particle swarm optimization algorithm," *Journal of Electromagnetic Waves and Applications*, Vol. 20, No. 13, 1785–1795, 2006.
13. Mallahzadeh, A. R., H. Oraizi, and Z. Davoodi-Rad, "Application of the invasive weed optimization technique for antenna configurations," *Progress In Electromagnetics Research*, PIER 79, 137–150, 2008.

14. Guo, J.-L., J.-Y. Li, and Q.-Z. Liu, "Analysis of antenna array with arbitrarily shaped radomes using fast algorithm based on VSIE," *Journal of Electromagnetic Waves and Applications*, Vol. 20, No. 10, 1399–1410, 2006.
15. Ayestarán, R. G., J. Laviada, and F. Las-Heras, "Synthesis of passive-dipole arrays with a genetic-neural hybrid method," *Journal of Electromagnetic Waves and Applications*, Vol. 20, No. 15, 2123–2135, 2006.
16. Zhang, Y. and W. Cao, "Array pattern synthesis based on weighted biorthogonal modes," *Journal of Electromagnetic Waves and Applications*, Vol. 20, No. 10, 1367–1376, 2006.
17. Chen, T. B., Y. L. Dong, Y. C. Jiao, and F. S. Zhang, "Synthesis of a circular antenna array using crossed particle swarm optimization algorithm," *Journal of Electromagnetic Waves and Applications*, Vol. 20, No. 13, 1785–1795, 2006.
18. Bucci, O. M., A. Capozzoli, and G. D'Elia, "An effective power synthesis technique for shaped, double-reflector multifeed antennas," *Progress In Electromagnetics Research*, PIER 39, 93–123, 2003.
19. Aziz, A., Q. Naqvi, and A. K. Hongo, "Analysis of the fields in two dimensional cassegrain system," *Progress In Electromagnetics Research*, PIER 71, 227–241, 2007.
20. Ghaffar, A., Q. A. Naqvi, and K. Hongo, "Analysis of the fields in three dimensional cassegrain system," *Progress In Electromagnetics Research*, PIER 72, 215–240, 2007.
21. Kraus, J. D., *Radio Astronomy*, 2nd Edition, Cygnus-Quasar Books, Ohio State University, Durham, 1986.
22. Kraus, J. D. and R. J. Marhefka, *Antennas for Applications*, Tata McGraw-Hill, New Delhi, 2003.
23. GMRT staff, et al., *Low Frequency Radio Astronomy*, 3rd edition, National Center for Radio Astrophysics, TIFR, Pune, 2007.
24. Troitskii, V. S., et al., "Calibration of the flux density of cassiopeia a and cygnus a in the range 300–9375 MHz," *Astronomicheskii Zhurnal*, Vol. 48, 1150, 1971.
25. Rohlfs, K. and T. L. Wilson, *Tools of Radio Astronomy*, 3rd edition, Springer-Verlag Berlin Heidelberg, 2000.
26. Karimkashi, S. and J. Rashed-Mohassel, "Sidelobe level reduction in symmetric dual-reflector antennas using a small lens antenna," *Journal of Electromagnetic Waves and Applications*, Vol. 20, No. 13, 1807–1816, 2006.